IEEE Access
Multidisciplinary | Rapid Review | Open Access Journal

Received August 29, 2019, accepted September 28, 2019, date of publication October 4, 2019, date of current version October 17, 2019.

Digital Object Identifier 10.1109/ACCESS.2019.2945563

Automated Brittle Fracture Rate Estimator for Steel Property Evaluation Using Deep Learning After Drop-Weight Tear Test

GYOGWON KOO[1], CRINO SHIN[2,3], HYEYEON CHOI[1], JONG-HAK LEE[4], SANG WOO KIM[1], AND JONG PIL YUN[2]

[1]Department of Electrical Engineering, Pohang University of Science and Technology, Pohang 37673, South Korea
[2]AI System Engineering Group, Korea Institute of Industrial Technology, Cheonan 31056, South Korea
[3]School of Electronics Engineering College of IT Engineering, Kyungpook National University, Daegu 41566, South Korea
[4]Technical Research Laboratories POSCO, Pohang 37859, South Korea

Corresponding authors: Sang Woo Kim (swkim@postech.edu) and Jong Pil Yun (rebirth@kitech.re.kr)

ABSTRACT This study proposes an automated brittle fracture rate (BFR) estimator using deep learning. As the demand for line-pipes increases in various industries, the need for BFR estimation through drop-weight tear test (DWTT) increases to evaluate steel's property. Conventional BFR or ductile fracture rate (DFR) estimation methods require an expensive 3D scanner. Alternatively, a rule-based approach is used with a single charge-coupled device (CCD) camera. However, it is sensitive to the hyper-parameter. To solve these problems, we propose an approach based on deep learning that has recently been successful in the fields of computer vision and image processing. The method proposed in this study is the first to use deep learning approach for BFR estimation. The proposed method consists of a VGG-based U-Net (VU-Net) which is inspired by U-Net and fully convolutional network (FCN). VU-Net includes a deep encoder and a decoder. The encoder is adopted from VGG19 and transferred with a pre-trained model with ImageNet. In addition, the structure of the decoder is the same as that of the encoder, and the decoder uses the feature maps of the encoder through concatenation operation to compensate for the reduced spatial information. To analyze the proposed VU-Net, we experimented with different depths of networks and various transfer learning approaches. In terms of accuracy used in real industrial application, we compared the proposed VU-Net with U-Net and FCN to evaluate the performance. The experiments showed that VU-Net was the accuracy of approximately 94.9 %, and was better than the other two, which had the accuracies of about 91.8 % and 93.7 %, respectively.

INDEX TERMS Computer vision, DWTT, industrial application, semantic segmentation, steel industry, transfer learning.

I. INTRODUCTION

Line-pipe has been widely used for long distance transportation of natural resources, such as crude oil and natural gas in extremely cold areas (e.g. Siberia and Alaska) [1], [2]. Hence, steels with excellent low-temperature toughness are required to manufacture these line-pipes. It is important to evaluate and manage the quality of these line-pipe steels, as well as steel productions from hot-rolling process.To evaluate the properties of steel, the drop-weight tear test (DWTT) has been widely used [3]–[6]. First developed at the Battelle Memorial Institute, USA, the DWTT is used to determine the fracture characteristics of pipelines and pressure vessels, and is an integral part of the material qualification programs for oil and gas, and other industrial applications. The ratio of the ductile and brittle fractures observed after the DWTT is strongly correlated with the resistance of the pipeline steels against brittle fracture propagation in the actual line-pipes. The test specimen is split up due to impact load by a hammer. The brittle fracture rate (BFR) or the ductile fracture rate (DFR) is determined by an operator to evaluate the specimen. Owing to the manual evaluation, which depends on the operator's condition and state of fatigue, reliability and reproducibility are not only degraded, but also the accuracy

The associate editor coordinating the review of this manuscript and approving it for publication was K. C. Santosh.

is not guaranteed. Furthermore, it is a time-consuming process. Therefore, the development of an automated evaluation system is essential to efficiently quantify the BFR and DFR from the DWTT.

Recently, many studies introduced various algorithms to evaluate and measure BFR and DFR of the DWTT specimens [7]–[9]. In [7], statistical methods and fractal concepts were used to evaluate the fracture surface of DWTT specimens. Multivariate characteristics of normal vectors in conjunction with the K-means clustering method were used in [8]. The inputs for the aforementioned algorithms were obtained by a 3D scanner. In [9], three input images were obtained from a single charge-coupled device (CCD) camera with different angles of illumination and then combined into a single image. The combined image was binarized into brittle and ductile fracture regions. However, the conventional algorithms require expensive devices or use hyper-parameter which could affect the performance of these algorithms.

Deep learning has lately shown great performance in a variety of fields such as industrial application [10]–[12], medical diagnosis [13], [14], agriculture [15] as well as imaging [16]. Semantic segmentation is one of the important tasks in field of the computer vision [17]–[19]. Unlike the classification and object detection tasks, the semantic segmentation task, which is also called as pixel-wise classification, is suitable for identifying and estimating the BFR.

To address the problems about conventional BFR or DFR estimation, we propose a novel automated evaluation system in this study. The proposed system is based on deep learning and images obtained from a CCD camera. The proposed network is inspired by U-Net [20] and fully convolutional network (FCN) [21]. We call the proposed network as 'VGG-based U-Net (VU-Net)'. By exploiting the architecture of U-Net, the proposed VU-Net has sufficient depth, and concatenates the feature maps of the encoder and the decoder to compensate for the loss of spatial information. Like in FCN, the transfer learning from VGG19, which was trained with a huge data (ImageNet), helps the network converge to an optimal point. When building networks for insufficient industrial data, bias-variance trade-off should be considered. In general, the deeper the network, the better its performance gets. However, the probability of over-fitting increases as the depth of the network increases. Therefore, we experimented on depth of network, as well as the transfer learning approaches, that help the network converge faster.

The main contributions of this study are summarized as follows.

- An automated evaluation system for BFR was proposed. It not only reduces the manpower and time costs involved but also performs a consistent evaluation.
- Unlike the conventional methods which used a 3D scanner, images for the surface of the broken specimens were obtained from a CCD camera. The equipment costs could be reduced.
- To the best of our knowledge, this study is the first to exploit a deep learning algorithm for BFR estimation.

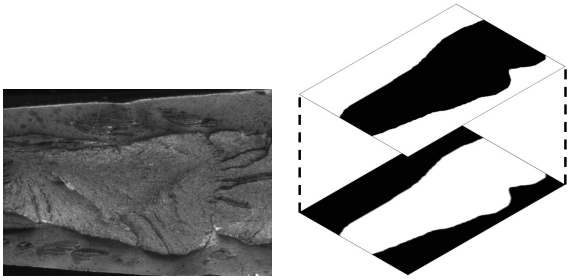

(a) (b)

FIGURE 1. Example of (a) an image after the DWTT and (b) its ground-truth data.

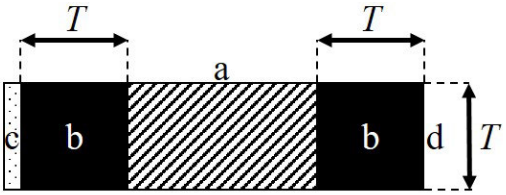

FIGURE 2. Image acquisition region for BFR or DFR estimation.

- To optimize VU-Net, we performed various experiments in terms of depth and transfer learning.
- The study was performed by images obtained from operators in situ to evaluate the surfaces of the broken specimens.

The remainder of this paper is organized as follows. In section II, the data and the BFR are explained. In section III, the proposed VU-Net for automated BFR estimation is presented. To analyze and evaluate VU-Net, various experiments were carried out in section IV. Finally, conclusions and future work are presented in section V.

II. DATA AND BRITTLE FRACTURE RATE (BFR)

Images of the broken specimen after the DWTT were obtained from a real industrial application. Both brittle and ductile fractures are revealed in Fig. 1a. The BFR or DFR is determined from the image excluded the thickness of the specimen in the notch area and the thickness of the specimen at the impact point of the hammer. In Fig. 2, the area denoted by **a** is the measurement or estimation region, and areas represented by **b** denote the excluded region. **c** and **d** are the notch area and the impact point of the hammer, respectively. T is the thickness of the specimen. Namely, the region denoted by **a** in Fig. 2 was acquired as the input for the network. To train a network, data pairs are required such as those in Fig. 1. Namely, a ground-truth data (GTD) corresponding to each image is needed such as Fig. 1b, where the pixel values of the white and black regions were 1 and 0, respectively. The GTD $\mathbf{g}_{hw}$ of input $\mathbf{x}_{hw}$ for $h = 1, \cdots, H$ and $w = 1, \cdots, W$ is defined as follows.

$$\mathbf{g}_{hw} = \begin{cases} \mathbf{v}_2 & \text{if } \mathbf{x}_{hw} \in \mathcal{R}_b \\ \mathbf{v}_1 & \text{otherwise,} \end{cases} \tag{1}$$

where W and H represent the width and height of the GTD (or the image), respectively. $\mathbf{v}_1$ and $\mathbf{v}_2$ are one-hot vectors

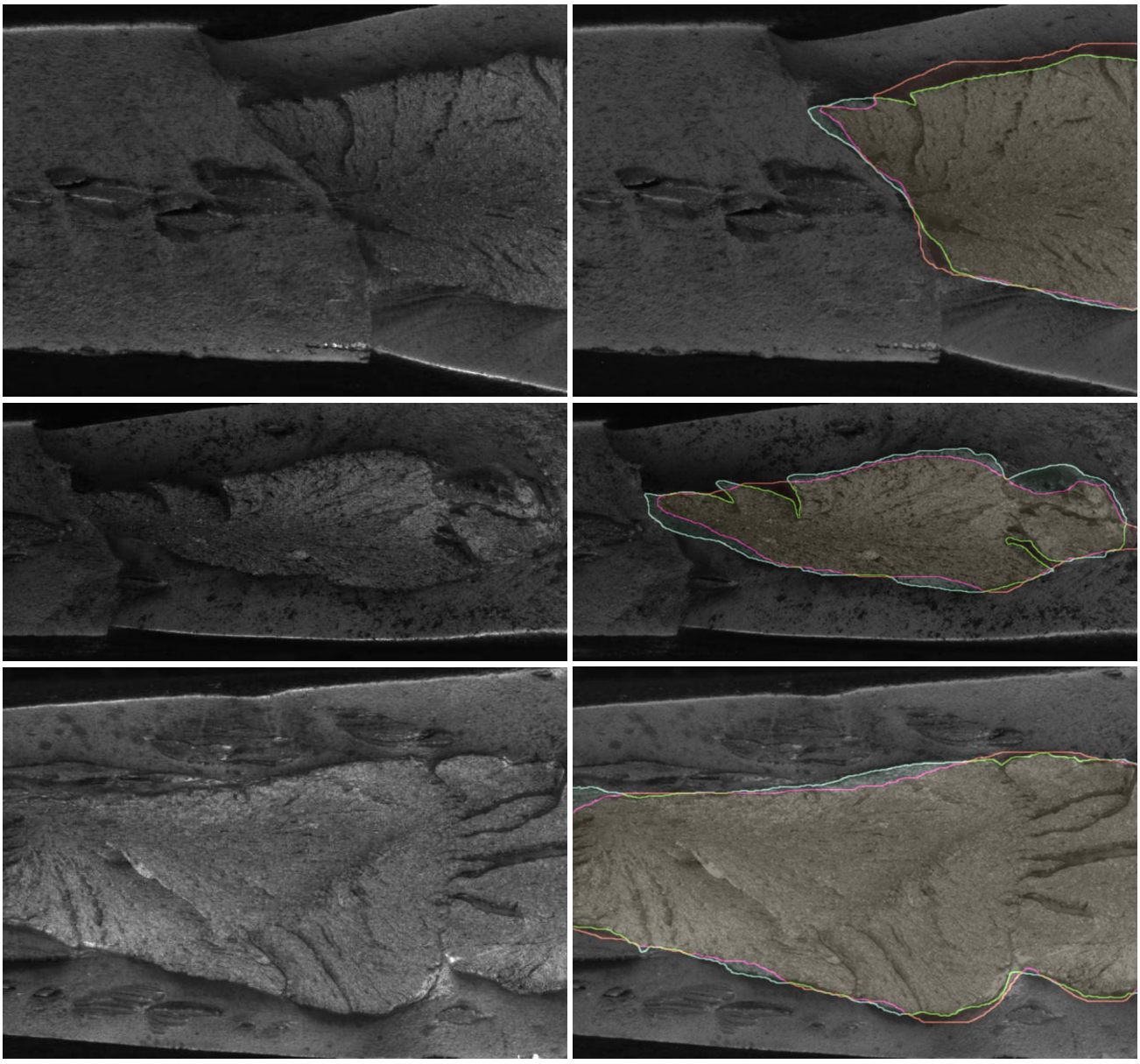

Image GTD refinement

FIGURE 3. Refinement of GTD for validation.

that assign 1 to only either the first or the second element. $\mathcal{R}_b$ represents the region of the brittle fracture in the image.

Our goal is to estimate the BFR $\mathcal{B}$, which is defined as follows.

$$\mathcal{B} = \frac{\sum_h \sum_w \mathbf{1}_{\mathbf{m}_{hw}=2}(\mathbf{m}_{hw})}{H \cdot W}, \tag{2}$$

where $\mathbf{1}_{\mathcal{K}}(x)$ denotes an indicator function, which is 1 if $x \in \mathcal{K}$ and 0 otherwise. $\mathbf{m}_{hw}$ is $\text{argmax}_c\, \mathbf{g}_{hw}$, where c is the channel of $\mathbf{g}_{hw}$. In other words, $\mathcal{B}$ is the ratio of the brittle fracture region to the total region of the target image.

To develop the automated BFR estimator, 1611 image and GTD pairs were obtained from a real industry site. The data set was approximately labeled for brittle fracture regions such as those enveloped by the red lines in Fig. 3. The networks could learn 'good representation' robustly because most regions of the noisy GTDs are correct [22]–[24]. Nevertheless, among them, 79 GTDs were made more elaborate than the rest of the GTDs to validate the networks. The brittle fracture regions of refined GTDs were labeled such as those enclosed by the green lines in Fig. 3. Re-labeling exquisitely the GTDs consume additional time, but the refined data plays an important role in determining the best model. Therefore, only a few images were allocated as the validation set and re-labeled elaborately. Finally, an additional 158 images were acquired for the test. The test set was used to analyze and evaluate networks.

III. AUTOMATED BRITTLE FRACTURE RATE ESTIMATOR

The automated BFR estimator is proposed by using deep learning approach in this study. One of the important tasks in

the field of computer vision is semantic segmentation which is also called as pixel-wise classification. It is suitable for the BFR estimation because the BFR is calculated by pixel in an image. In general, a deep learning network for semantic segmentation consists of an encoder and a decoder [21], [20], [25]. The encoder extracts high-dimensional features from the surface image of a broken specimen. In terms of the architecture and the role, the encoder is similar to the feature extractor of conventional convolutional neural networks (CNNs) such as VGGNet [26] and ResNet [27]. The famous CNNs extract good representation by training with ImageNet which has a large data set [28]. Therefore, many studies used the pre-trained models as initial values of the networks to accelerate their convergence in semantic segmentation tasks [17], [21], [25], [29]. The decoder generates the segmented output from the features of the encoder. When the features are extracted in the encoder, the spatial information is shrunk. To compensate for this problem, fusion operation is applied in the decoder. The fusion operation concatenates or adds the feature map of the encoder to the feature map of the decoder. Here, the concatenation is a channel connection, and the addition is an element-wise sum. Therefore, for the former, two feature maps should be the spatially same. For the latter, two feature maps should be the same size including channel.

The proposed VU-Net was shown in Fig. 4, where $C_{a,b}$, R, Max, d and $D_{a,s,b}$ represent the convolution layer, ReLU (Rectified Linear Unit) operation, max pooling layer, dropout operation and deconvolution layer, respectively. The subscripts a, b and s are the kernel size ($a \times a$), the number of kernels and the stride, respectively. As fusion operation, cc represents the concatenation of the feature maps of the encoder, connected by dashed arrows, to the input of cc. For example, feeding an input to $C_{a,b} \cdot R \cdot d$ box means that the input is applied in turn to a convolution layer with b $a \times a$ kernels, a ReLU operation and a dropout operation. The proposed encoder was based on VGG19 model to achieve sufficient depth and transfer learning, and the proposed decoder was a twin of the encoder except for the last convolution layer block. The convolution layer block was defined as 2-4 convolution layers between the max pooling layers. In the encoder, the last outputs of the convolution layer blocks were used for fusion operation.

IV. EXPERIMENT

The flowchart of experiments was shown in Fig. 5. According to the flowchart, we conducted various experiments for the depth of the proposed network and transfer learning. All experiments were performed with Intel core i7-6700K CPU, 32 *GB* RAM and Nvidia Titan X Pascal GPU. Cross-entropy was used as the loss function $\mathcal{L}$ as follows.

$$\mathcal{L} = -\frac{1}{H \cdot W} \sum_{h} \sum_{w} \mathbf{g}_{hw} \log \hat{\mathbf{g}}_{hw}, \tag{3}$$

where $\hat{\mathbf{g}}_{hw}$ represents the output of the network. In this study, networks were trained by stochastic gradient descent method

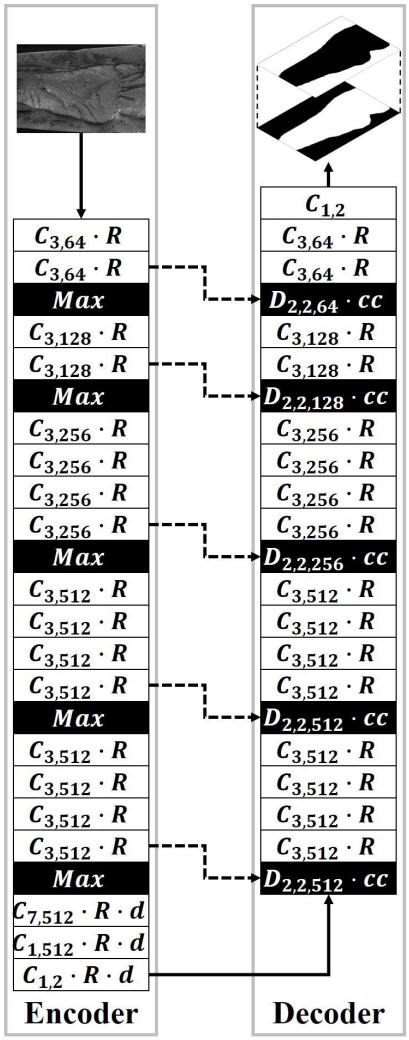

FIGURE 4. Architecture of VU-Net.

with Adam optimizer. The initial learning rate was set to 0.0001, which decayed 5 % per epoch, where one epoch means when an entire train set is passed through the neural network only once. Inputs of networks are 8-bit gray level and vary in width and height as shown in Table 1 because of different sizes of the specimens. To focus patterns of brittle and ductile fracture regions, all inputs of the networks were normalized from 0 to 1 by unity-based normalization also known as min-max normalization. This normalization is helped to improve the performance of networks [30], [31] and defined as follows.

$$\tilde{\mathbf{x}}_{hw} = \frac{\mathbf{x}_{hw} - min(\mathbf{X})}{max(\mathbf{X}) - min(\mathbf{X})}, \tag{4}$$

$$\mathbf{X} = \{\mathbf{x}_{hw} | h = 1, \cdots, H, \ w = 1, \cdots, W\}, \tag{5}$$

where $\tilde{\mathbf{x}}_{hw}$ represents normalized input $\mathbf{x}_{hw}$. $min(\mathbf{X})$ and $max(\mathbf{X})$ are minimum and maximum values of input $\mathbf{X}$, respectively. These experimental details were summarized in Table 2.

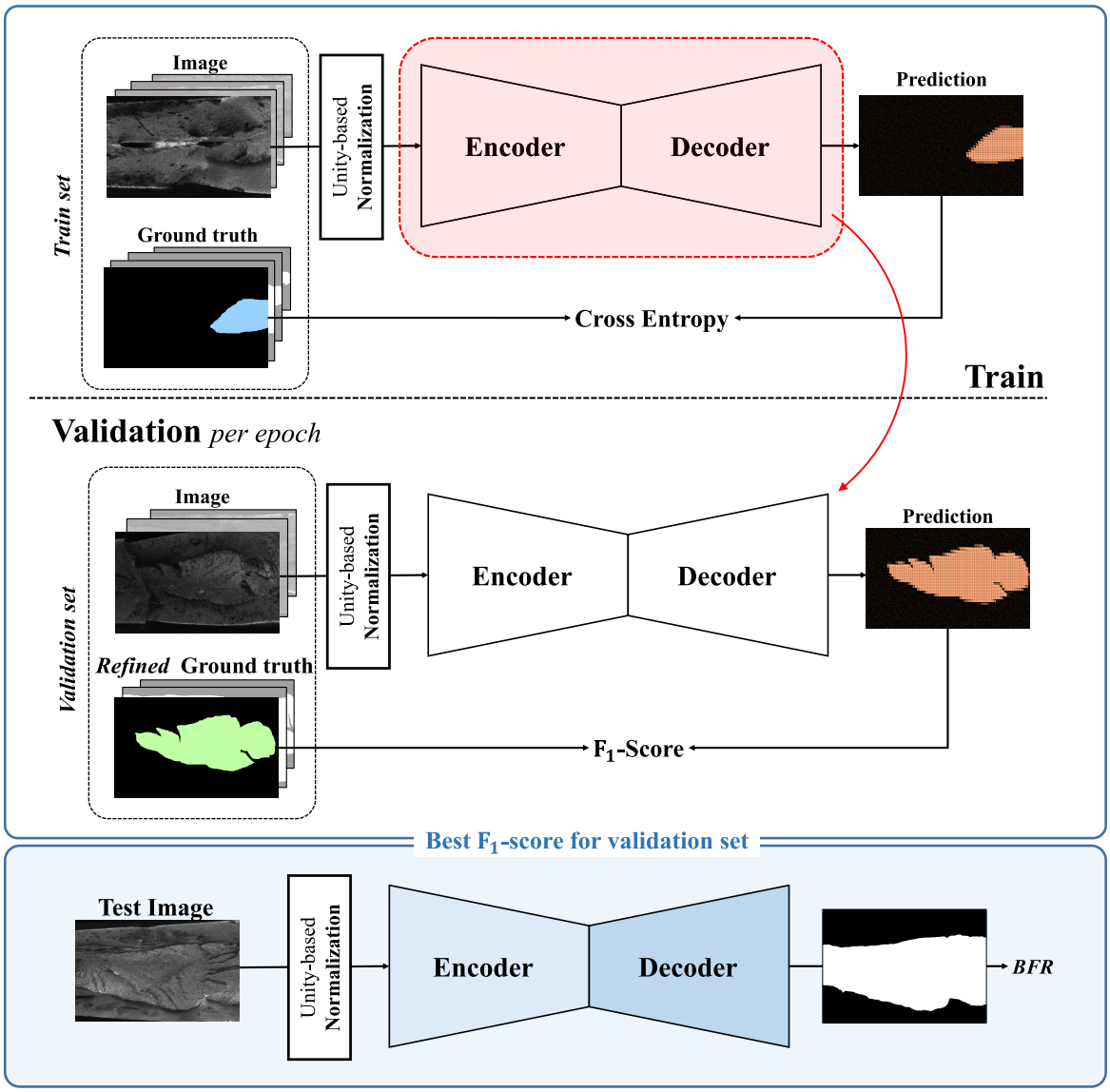

FIGURE 5. Flowchart for experimental details.

TABLE 1. Size information and statistics data of the broken specimen images.

	Mean	SD	Min	Max
Width	625.82	22.32	611	810
Height	462.65	93.21	262	676

We used two indices to evaluate the performance of the networks.

- F_1-score F_1

$$F_1 = 2 \cdot \frac{Pre \cdot Sen}{Pre + Sen} \times 100, \tag{6}$$

where *Pre* and *Sen* are the precision and the sensitivity, respectively. The precision is the fraction of the true brittle fracture pixels in the predicted brittle fracture pixels. The sensitivity is the fraction of correctly predicted brittle fracture pixels in the total true brittle fracture pixels. F_1-score is a harmonic average of the precision and the sensitivity.

- Accuracy $\mathcal{A}$

$$\mathcal{A} = \frac{1}{N} \sum_{n}^{N} \mathbf{1}_{\mathbf{p}^n \le t}(\mathbf{p}^n) \times 100, \tag{7}$$

$$\mathbf{p}^n = \left| \mathcal{B}^n - \hat{\mathcal{B}}^n \right|, \tag{8}$$

$$\hat{\mathcal{B}}^n = \frac{\sum_h \sum_w \mathbf{1}_{\hat{\mathbf{m}}^n_{hw}=2}(\hat{\mathbf{m}}^n_{hw})}{H \cdot W}, \tag{9}$$

$$\hat{\mathbf{m}}^n_{hw} = \text{argmax}_c \, \hat{\mathbf{g}}^n_{hw} \quad \text{for } c = 1, 2, \tag{10}$$

where the superscript n means the n^{th} target image. N represents the size of the test set. $\hat{\mathbf{g}}^n_{hw}$ is the output vector of (h, w) coordinate for the n^{th} target image. In other words, accuracy means the fraction of the number of correct estimations over N. An estimation is correct if

TABLE 2. Summary of common details of the experiments.

Experimental details	
Loss function	Cross-entropy
Optimizer	ADAM optimizer
Learning rate	$0.0001 \times 0.95^{epoch-1}$
Input	Surface image of broken specimen after DWTT
Data set	Train:Validation:Test $= 1532 : 79 : 158$
Input normalization	Unity-based normalization (Min-max normalization)

the absolute error of the estimated BFR is less than t. In this study, t was set to 0.05 because there is a 5 % margin of BFR estimation in the real industry.

F_1-score evaluates the pixel-wise estimation of the networks, and the accuracy $\mathcal{A}$ evaluates the BFR estimation of the networks. The dropout rate was empirically determined for each network. In each network frame, the model, which had the best F_1-score for validation set, was selected and tested.

A. DEPTH OF VU-NET

To analyze the performance of VU-Net with regard to its depth, experiments for four different depths were performed (see Table 3). VU-Net-19 is shown in Fig. 4, where 19 is the number of convolution layers of the encoder. For VU-Net-16, VU-Net-12, and VU-Net-10, the last 3, 7 and 9 convolution layers, respectively, of the encoder were eliminated together with the max pooling layers. In addition, the corresponding convolution layers and deconvolution layers of the decoder were also removed. Because VGG19 has 16 convolution layers, the first 16 convolution layers of the encoder were initialized with VGG19, and the others were initialized with a truncated normal distribution. The initialization of the networks and the transfer learning will be explained, in detail, in the next subsection.

The result is shown in Table 3. VU-Net-16 showed the best F_1-score and accuracy. In other words, the result said that VU-Net-16 has the optimal depth for BFR estimation. Therefore, we used the architecture of VU-Net-16 in the next experiments.

B. TRANSFER LEARNING OF VU-NET

Next, we experimented with four options to analyze the transfer learning of VU-Net. The four options for transfer learning are as follows.

1) No transfer: VU-Net was initialized with values generated by a truncated normal distribution. The generated value followed a normal distribution with mean ($\mu = 0$) and standard deviation ($\sigma = 0.02$), but this value was dropped and re-picked if its magnitude was more or less 2σ than μ.
2) Transfer encoder & Fix: 'Fix' relates to fixing the weights of the transferred part. The first 12 convolution layers of the encoder were transferred by pre-trained VGG19 and fixed. The reason was to apply the dropout operation in the last convolution layer block of the encoder. The rest were initialized with values generated by the truncated normal distribution and trained.
3) Transfer encoder & FT: 'FT' stands for fine tuning. The first 16 convolution layers of the encoder were transferred from VGG19, and the rest were initialized with values generated by the truncated normal distribution. Next, all layers of VU-Net were trained together.
4) Transfer all & FT: The encoder was transferred equivalently as in 3). The decoder was also initialized by VGG19, and then, both parts were trained together. If the channels of the input and the output were different, a 1×1 convolution layer was added. This approach is possible because the structures of the encoder and the decoder are twins.

TABLE 3. Performance comparison of VU-Net based on depth.

Network	F_1-score	Accuracy
VU-Net-10	95.1897	91.7722
VU-Net-12	95.4724	93.038
VU-Net-16	**95.5561**	**94.9367**
VU-Net-19	95.3959	93.038

TABLE 4. Performance comparison of the transfer learning.

Transfer option	F_1-score	Accuracy
No transfer	94.3119	86.0759
Transfer encoder & Fix	94.8858	92.4051
Transfer encoder & FT	**95.5561**	**94.9367**
Transfer all & FT	95.5306	93.6709

The results are shown in Table 4. Firstly, the results show that the transfer learning was effective. The reason is why the pre-trained model was already trained with big data to extract good features. Secondly, fine tuning was necessary for the optimization. Finally, the weights of the classifier should be transferred into only the encoder as the feature extractor.

C. PERFORMANCE COMPARISON FOR BFR ESTIMATION

In this experiment, VU-Net was compared with conventional semantic segmentation methods such as FCN and U-Net. The performance of VU-Net is shown in Table 5. To show the performance of the encoder, VU-Net was also compared with FCN and VU-Net based on ResNet [27]. ResNet consists of 5 convolution layer blocks. Based on the output's size of

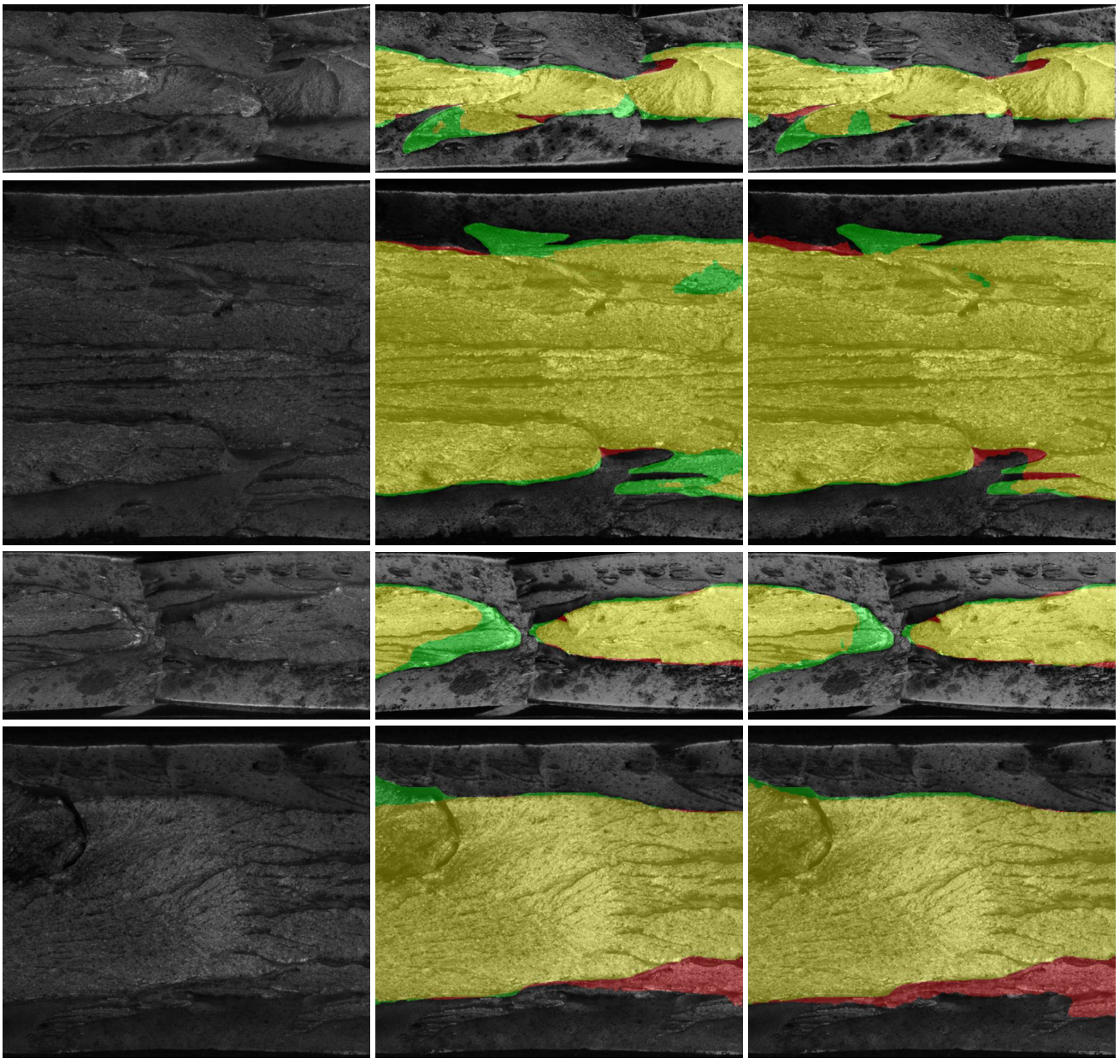

FIGURE 6. **Comparison between the results of FCN and VU-Net.**

the convolution layer block, we added deconvolution layers and fusion operation in the decoder. In the case of VU-Net based on ResNet, the last fusion operation was omitted because the first convolution layer block is ambiguous [27]. In terms of F_1-score and accuracy, VU-Net performed better than the conventional networks, and VGG19 was more appropriate than ResNet as an encoder. F_1-score did not differ much, but accuracy was much different. The reason is why, for entire images, the brittle fracture regions were similarly segmented, but for an individual image, VU-Net segmented better brittle fracture region than the other networks. Therefore, VU-Net was more suitable for estimating the BFR than the others. Four examples of BFR estimation are shown in Fig. 6 to compare the performance of VU-Net and FCN based on VGG19. The green and red regions represent true and estimated brittle regions, respectively. The yellow region is an overlap of the true and the estimated brittle regions. In the first three examples, VU-Net performed better for BFR estimation than FCN. On the other hand, the fourth example was the opposite. However, in the fourth example of Fig. 6, it may be noticed that the estimation faults (red regions) of the two networks were somewhat similar, but there was more green region in FCN results than in VU-Net results.

TABLE 5. Performance comparison of FCN, U-Net, and VU-Net.

Network (pre-trained model)	F_1-score	Accuracy
FCN (ResNet50)	94.7044	89.8734
VU-Net (ResNet50)	94.8538	91.1392
U-Net [20]	94.6479	91.7722
FCN (VGG19) [21]	95.2232	93.6709
VU-Net (VGG19)	**95.5561**	**94.9367**

V. CONCLUSION

As the use of steel, such as line-pipes, increases, the importance of analyzing DWTT's results increases for quality management. Conventional methods have the disadvantage of requiring expensive equipment or being very vulnerable to change of user parameters. Therefore, we proposed an automated BFR estimator based on deep learning. The proposed network, which called as VU-Net, was inspired by the architectures of U-Net and FCN. The encoder of VU-Net reflected VGG19, which is powerful and easy classifier. The decoder of VU-Net was a mirror of the encoder, and was applied fusion operation. VU-Net was variously analyzed to configure the proper architecture for the BFR estimation. VU-Net-16, which had 16 convolution layers in the encoder, was best performance among the VU-Nets of different depths. In addition, we experimented with various transfer learning approaches to extract good representation. The best approach was the one where the encoder was initialized with a pre-trained model and the entire network (both the encoder and decoder) was fine-tuned. The accuracy of this approach was about 8.9 % higher than without transfer learning. Finally, we compared VU-Net with FCN and U-Net. In terms of F_1-score and accuracy, VU-Net yielded better performance than the others. Based on the proposed VU-Net, an automated system for BFR estimation not only reduces money, human and time costs but also makes a consistent decision for steel's quality.

Furthermore, when applying deep learning to real industrial sites, it has been difficult to obtain quantitatively and qualitatively sufficient data with labels. These problems limit the performance. In the future, it is necessary to study algorithms and systems to compensate for these problems.

REFERENCES

[1] B. Hwang, Y. M. Kim, S. Lee, N. J. Kim, and J. Y. Yoo, "Correlation of rolling condition, microstructure, and low-temperature toughness of x70 pipeline steels," *Metall. Mater. Trans. A*, vol. 36, no. 7, pp. 1793–1805, 2005.

[2] Y.-P. Zeng, P.-Y. Zhu, and K. Tong, "Effect of microstructure on the low temperature toughness of high strength pipeline steels," *Int. J. Minerals, Metall., Mater.*, vol. 22, no. 3, pp. 254–261, 2015.

[3] B. Hwang, S. Lee, Y. M. Kim, N. J. Kim, J. Y. Yoo, and C. S. Woo, "Analysis of abnormal fracture occurring during drop-weight tear test of high-toughness line-pipe steel," *Mater. Sci. Eng., A*, vol. 368, nos. 1–2, pp. 18–27, 2004.

[4] Z. Yang, C.-B. Kim, Y. Feng, and C. Cho, "Abnormal fracture appearance in drop-weight tear test specimens of pipeline steel," *Mater. Sci. Eng., A*, vol. 483, pp. 239–241, Jun. 2008.

[5] S. Hong, S. Y. Shin, S. Lee, and N. J. Kim, "Effects of specimen thickness and notch shape on fracture modes in the drop weight tear test of api x70 and x80 linepipe steels," *Metall. Mater. Trans. A*, vol. 42, no. 9, pp. 2619–2632, 2011.

[6] D. L. Rudland, Y.-Y. Wang, G. Wilkowski, and D. J. Horsley, "Characterizing dynamic fracture toughness of linepipe steels using the pressed-notch drop-weight-tear test specimen," *Eng. Fract. Mech.*, vol. 71, nos. 16–17, pp. 2533–2549, 2004.

[7] B. Strnadel, P. Ferfecki, and P. Židlík, "Statistical characteristics of fracture surfaces in high-strength steel drop weight tear test specimens," *Eng. Fract. Mech.*, vols. 112–113, pp. 1–13, Nov. 2013.

[8] P. Skalny, "Evaluation and identifying the ductile fracture area of x70 steel from DWTT broken specimens," *Procedia Struct. Integrity*, vol. 2, pp. 3727–3734, 2016.

[9] T.-S. Kim and S.-G. Park, "A study on decision algorithm of ductile-brittle rates of DWTT specimens of API linepipe steels," in *Proc. Int. Conf. Future Inf. Commun. Eng.*, 2015, vol. 7, no. 1, pp. 505–508.

[10] H. Yan, J. Wan, C. Zhang, S. Tang, Q. Hua, and Z. Wang, "Industrial big data analytics for prediction of remaining useful life based on deep learning," *IEEE Access*, vol. 6, pp. 17190–17197, 2018.

[11] J. Pan, Y. Yin, J. Xiong, W. Luo, G. Gui, and H. Sari, "Deep learning-based unmanned surveillance systems for observing water levels," *IEEE Access*, vol. 6, pp. 73561–73571, 2018.

[12] Z.-W. Xu, X.-M. Liu, and K. Zhang, "Mechanical properties prediction for hot rolled alloy steel using convolutional neural network," *IEEE Access*, vol. 7, pp. 47068–47078, 2019.

[13] N. Brancati, G. De Pietro, M. Frucci, and D. Riccio, "A deep learning approach for breast invasive ductal carcinoma detection and lymphoma multi-classification in histological images," *IEEE Access*, vol. 7, pp. 44709–44720, 2019.

[14] T. A. Soomro, A. J. Afifi, L. Zheng, S. Soomro, J. Gao, O. Hellwich, and M. Paul, "Deep learning models for retinal blood vessels segmentation: A review," *IEEE Access*, vol. 7, pp. 71696–71717, 2019.

[15] P. Jiang, Y. Chen, B. Liu, D. He, and C. Liang, "Real-time detection of apple leaf diseases using deep learning approach based on improved convolutional neural networks," *IEEE Access*, vol. 7, pp. 59069–59080, 2019.

[16] Y. Wang, L. Wang, H. Wang, and P. Li, "End-to-end image super-resolution via deep and shallow convolutional networks," *IEEE Access*, vol. 7, pp. 31959–31970, 2019.

[17] G. Koo, J. P. Yun, S. J. Lee, H. Choi, and S. W. Kim, "End-to-end billet identification number recognition system," *ISIJ Int.*, vol. 59, no. 1, pp. 98–103, 2019.

[18] M. Wu, C. Zhang, J. Liu, L. Zhou, and X. Li, "Towards accurate high resolution satellite image semantic segmentation," *IEEE Access*, vol. 7, pp. 55609–55619, 2019.

[19] R. Dong, X. Pan, and F. Li, "DenseU-Net-based semantic segmentation of small objects in urban remote sensing images," *IEEE Access*, vol. 7, pp. 65347–65356, 2019.

[20] O. Ronneberger, P. Fischer, and T. Brox, "U-net: Convolutional networks for biomedical image segmentation," in *Proc. Int. Conf. Med. Image Comput. Comput.-Assist. Intervent.* Berlin, Germany: Springer, 2015, pp. 234–241.

[21] J. Long, E. Shelhamer, and T. Darrell, "Fully convolutional networks for semantic segmentation," in *Proc. IEEE Conf. Comput. Vis. Pattern Recognit.*, Jun. 2015, pp. 3431–3440.

[22] S. Reed, H. Lee, D. Anguelov, C. Szegedy, D. Erhan, and A. Rabinovich, "Training deep neural networks on noisy labels with bootstrapping," 2014, *arXiv:1412.6596*. [Online]. Available: https://arxiv.org/abs/1412.6596

[23] J. Krause, B. Sapp, A. Howard, H. Zhou, A. Toshev, T. Duerig, J. Philbin, and L. Fei-Fei, "The unreasonable effectiveness of noisy data for fine-grained recognition," in *Proc. Eur. Conf. Comput. Vis.* Berlin, Germany: Springer, 2016, pp. 301–320.

[24] C. Sun, A. Shrivastava, S. Singh, and A. Gupta, "Revisiting unreasonable effectiveness of data in deep learning era," in *Proc. IEEE Int. Conf. Comput. Vis.*, Oct. 2017, pp. 843–852.

[25] L.-C. Chen, G. Papandreou, F. Schroff, and H. Adam, "Rethinking atrous convolution for semantic image segmentation," 2017, *arXiv:1706.05587*. [Online]. Available: https://arxiv.org/abs/1706.05587

[26] K. Simonyan and A. Zisserman, "Very deep convolutional networks for large-scale image recognition," 2014, *arXiv:1409.1556*. [Online]. Available: https://arxiv.org/abs/1409.1556

[27] K. He, X. Zhang, S. Ren, and J. Sun, "Deep residual learning for image recognition," in *Proc. IEEE Conf. Comput. Vis. Pattern Recognit.*, Jun. 2016, pp. 770–778.
[28] J. Deng, W. Dong, R. Socher, L.-J. Li, K. Li, and L. Fei-Fei, "ImageNet: A large-scale hierarchical image database," in *Proc. IEEE Conf. Comput. Vis. Pattern Recognit.*, Jun. 2009, pp. 248–255.
[29] A. A. Shvets, A. Rakhlin, A. A. Kalinin, and V. I. Iglovikov, "Automatic instrument segmentation in robot-assisted surgery using deep learning," in *Proc. 17th IEEE Int. Conf. Mach. Learn. Appl. (ICMLA)*, Dec. 2018, pp. 624–628.
[30] S. Ryu, H. Choi, H. Lee, H. Kim, and V. W. S. Wong, "Residential load profile clustering via deep convolutional autoencoder," in *Proc. IEEE Int. Conf. Commun., Control, Comput. Technol. Smart Grids (SmartGridComm)*, Oct. 2018, pp. 1–6.
[31] A. Ntakaris, G. Mirone, J. Kanniainen, M. Gabbouj, and A. Iosifidis, "Feature engineering for mid-price prediction with deep learning," *IEEE Access*, vol. 7, pp. 82390–82412, 2019.

GYOGWON KOO received the B.S. degree from the Department of Electrical Engineering, Kyungpook National University, Daegu, South Korea, in 2013, and the M.S. degree from the Department of Electrical Engineering, Pohang University of Science and Technology, Pohang, South Korea, in 2015, where he is currently pursuing the Ph.D. degree with the Department of Electrical Engineering.

His current research interests include computer vision and deep learning.

CRINO SHIN received the B.S. degree in electronic engineering from Kyungpook National University, South Korea, in 2017, where he is currently pursuing the M.S. degree in electronic engineering. He is also currently pursuing the degree with the Korea Institute of Industrial Technology.

His research interests include deep learning and computer vision.

HYEYEON CHOI received the B.S. and M.S. degrees in electrical engineering from the Pohang University of Science and Technology (POSTECH), Pohang, South Korea, in 2017 and 2019, respectively, where she is currently pursuing the Ph.D. degree in electrical engineering. Her research interests include computer vision and deep learning applications.

JONG-HAK LEE received the Ph.D. degree in electrical engineering from Kyungpook National University, in 2005. He is currently a Senior Principal Researcher with the POSCO Lab. His research interests include system engineering, defect classification using machine vision, image processing, and deep neural networks.

SANG WOO KIM received the B.S., M.S., and Ph.D. degrees from the Department of Control and Instrumentation Engineering, Seoul National University, Seoul, South Korea, in 1983, 1985, and 1990, respectively.

In 1992, he joined the Pohang University of Science and Technology, Pohang, South Korea, as an Assistant Professor, where he is currently a Full Professor with the Department of Electrical Engineering. In 1993, he was a Visiting Fellow of the Department of Systems Engineering, Australian National University, Canberra, ACT, Australia. His current research interests include optimal control, optimization algorithms, intelligent control, wireless communication, and process automation.

JONG PIL YUN received the Ph.D. degree in electrical engineering from the Pohang University of Science and Technology, in 2009. He is currently a Principal Researcher with the Korea Institute of Industrial Technology. His research interests include defect detection, classification using machine vision, image processing, and deep neural networks.